Journal of Materials Chemistry A



PAPER

View Article Online
View Journal | View Issue



Cite this: *J. Mater. Chem. A*, 2015, **3**, 2617

# Photocatalytic degradation of organic pollutants by shape selective synthesis of β-$Ga_2O_3$ microspheres constituted by nanospheres for environmental remediation

K. Girija,*[ac] S. Thirumalairajan,[b] Valmor R. Mastelaro[b] and D. Mangalaraj[a]

Received 5th October 2014
Accepted 7th December 2014

DOI: 10.1039/c4ta05295a

www.rsc.org/MaterialsA

A potential single crystalline photocatalyst β-$Ga_2O_3$ with unique spherical morphology has been synthesized using a surfactant assisted hydrothermal process. Organic additive triblock co-polymer pluronic F127 was used as a soft template. The morphology of the material was investigated using scanning electron microscopy and it was confirmed that the nanospheres self-assembled to form microspheres with diameters in the range ~1–3 μm. The crystal phase and chemical composition of the β-$Ga_2O_3$ microspheres were revealed by X-ray diffraction and X-ray photoelectron spectroscopy. Structural characterization exhibits the monoclinic phase of the microspheres with preferential growth along the [111] direction. A plausible mechanism has been proposed to understand the formation of microspheres. The optical absorbance spectrum showed an intense absorption feature in the UV spectral region with a bandgap energy of 4.6 eV. The Brunauer–Emmett–Teller specific surface area was found to be 82 $m^2\ g^{-1}$. The photocatalytic activity of the material has been investigated for the degradation of model organic pollutants Rhodamine B and methylene blue under ultraviolet light irradiation. The photocatalytic mechanism towards the degradation of organic dyes has also been proposed.

## 1 Introduction

Earlier research activities emphasized mainly the control of the stoichiometry of products, however with the development of nanotechnology considerable effort has been put forth to control the morphology and size.[1] Nanostructures as functional building blocks are ideal candidates for the investigation of the dependence of structural, morphological and optical properties on the quantum confinement effect, which paves way for novel nanotechnological applications.[2,3] Both the physical and chemical properties of nanostructures are associated with their size, shape and dimensionality; therefore morphology-controlled synthesis of functional nanostructures gains importance from a scientific and technological perspective.[4] The precise control of the growth of nanomaterials allows a higher level of selectivity, control over dimensionality and morphology, and the possibility of incorporating these nanostructures into nanotechnological devices. There is an increasing interest in pursuing effective synthesis strategies for the fabrication of advanced materials with complex shapes and hierarchical organization. Synthesis of inorganic semiconducting β-$Ga_2O_3$ nanostructures have gained interest in materials science due to their potential applications in optoelectronics, such as waveguides and optical emitters for UV radiation, solar cells, gas sensing and, recently, as photocatalysts.[5,6] In order to grow β-$Ga_2O_3$ nanostructures, wet chemical approaches such as the reflux condensation method, sol–gel, hydrothermal processes and precipitation techniques have been employed.[7–11] Different nanostructures can be synthesized *via* hydrothermal process due to their obvious advantages such as being economically cheap, efficient and environment friendly for the production of the desired phase in a very short time using simple equipment. However, to control the morphology, structure and properties, the surfactant-assisted hydrothermal method has elicited great interest, due to its significant advantages such as controlled size, low temperature growth, tunable shape and less-complicated processes . The properties of the β-$Ga_2O_3$ nanostructures depend on the preparation method, which in turn plays an important role in their potential application.

Semiconductor-mediated photocatalysts can degrade a wide range of organic contaminants like Rhodamine B, methylene blue, Congo red, *etc.*,[12] for photocatalysis applications; it has been reported that β-$Ga_2O_3$ exhibits high and stable photocatalytic activity over commercial $TiO_2$ due to the strong redox ability of photogenerated electron–hole pairs.[13–15] Meanwhile,

[a]*Department of Nanoscience and Technology, Bharathiar University, Coimbatore-641 046, India. E-mail: kgirija.bu@gmail.com; Fax: +91 422 2369106; Tel: +91 422 2369130*

[b]*Instituto de Física de São Carlos (IFSC), University de São Paulo, CP 369, 13560-970 São Carlos, SP, Brazil*

[c]*Department of Science and Humanities, Dr N.G.P. Institute of Technology, Coimbatore-641 048, India*

different phases of $Ga_2O_3$ with nano/microstructures such as belts, wires and rods have been confirmed to possess extraordinary photocatalytic ability to photodegrade RhB and Acid Orange 7, and reduce Cr(VI) and methylene blue under exposure to ultraviolet (UV) light irradiation.[16–20]

Herein, we report for the first time the synthesis of β-$Ga_2O_3$ spherical assemblies by surfactant assisted hydrothermal processing and their potential involvement in the photocatalytic degradation of organic pollutants Rhodamine B and Methylene blue under UV light. The photocatalytic mechanism of β-$Ga_2O_3$ microspheres towards organic dye has also been discussed to demonstrate their potential environment application.

# 2 Materials and method

## 2.1 Sample preparation

For the preparation of β-$Ga_2O_3$ microspheres by the surfactant assisted hydrothermal method, $Ga(NO_3)_3 \cdot nH_2O$ and the structure directing agent pluronic F127 were used as starting materials. All the chemicals were of analytical pure grade (99.99%) and used without further purification. In the typical synthesis process, gallium nitrate (0.01 mol $L^{-1}$) and a stoichiometric amount of surfactant F127 were dissolved in double distilled water under magnetic stirring. The precursor solution was stirred continuously for about an hour. The optimized molar amount of surfactant to $Ga^{3+}$ was 1 : 5. The resultant solution was then transferred into a 40 mL Teflon-lined stainless steel autoclave for hydrothermal treatment maintained at 180 °C for 12 h. The autoclave was cooled down to room temperature naturally after hydrothermal treatment. The obtained products were separated by centrifugation, washed repeatedly with alcohol and distilled water to remove the unreacted ions, by-products and organic impurities if present in the product, followed by drying at 100 °C and calcination at 900 °C for 3 h to obtain white powder samples of β-$Ga_2O_3$.

## 2.2 Characterization techniques

The products obtained at various stages of the chemical reaction were systematically characterized using different techniques. The surface morphology and structure of the prepared spherical β-$Ga_2O_3$ was characterized using scanning electron microscopy (SEM, JEOL JSM-6380LV) and X-ray diffraction technique (XRD, Bruker Germany D8 Advance) with $CuK_{\alpha 1}$ radiation ($\lambda$ = 1.54 Å). In-depth surface morphology images were recorded using transmission electron microscopy (TEM) employing a JEOL JEM 2000 Fx-11 at an acceleration voltage of 200 kV. X-ray photoelectron spectroscopy (XPS) measurements were performed using ESCA + Omicron UK XPS system with an $MgK_{\alpha}$ source and photon energy 1486.6 eV. All the binding energies were referenced to the C 1s peak at 284.6 eV of the surface adventitious carbon. Fourier-transform infrared (FTIR) spectroscopy was performed on a Thermo Nicolet 200 FTIR spectrometer using the KBr wafer technique. The spectrum was collected in the mid-IR range from 400 to 4000 $cm^{-1}$ with a resolution of 1 $cm^{-1}$. The UV-Vis diffuse reflectance spectrum was obtained using a Shimadzu UV-2401PC spectrophotometer. Nitrogen adsorption–desorption isotherms were obtained using a Belsorp HP surface area analyzer at 77 K. Prior to measurement, the samples were degassed at 393 K for 12 h.

## 2.3 Photocatalytic reaction

The photocatalytic activity of β-$Ga_2O_3$ microspheres for the decolorization of Rhodamine B (RhB) and Methylene Blue (MB) in aqueous solution under ultraviolet light irradiation was evaluated by measuring the absorbance of the irradiated solution. Prior to irradiation, 50 mg photocatalyst was mixed with RhB (50 mL, with a concentration of $2 \times 10^{-5}$ M) in a 100 mL round-bottomed flask. In the case of MB, 50 mg of photocatalyst was added to 50 mL of aqueous MB solution. In separate experiments, the suspension was magnetically stirred in the dark to reach a complete adsorption–desorption equilibrium of RhB and MB on the catalyst surface. The suspensions were then illuminated using a 150 W xenon lamp source. An aliquot of 3 mL was taken from the multi lamp photocatalyst reactor at regular intervals of 30 min to be analyzed by UV-Vis spectroscopy (Lambda 35, Perkin-Elmer). Duplicate runs were carried out for each condition and the optimized results are presented.

# 3 Results and discussion

## 3.1 Morphology analysis

The low and high magnified SEM images of the β-$Ga_2O_3$ (Fig. 1a and b) prepared using triblock co-polymer pluronic F127 shows the formation of microspheres with pores on their surface. A panoramic view of the SEM images shows the abundant yield of β-$Ga_2O_3$ microspheres obtained through a hydrothermal process at 180 °C for 12 h. The formed microspheres are well dispersed but they lack uniformity in terms of their size.

The diameter of the microspheres ranges from ~1 to 3 μm. It should be mentioned that such a novel morphology has not been reported for β-$Ga_2O_3$ previously through the surfactant assisted hydrothermal technique. Through the synthesis technique used in the present study, it was possible to tune the shape of the β-$Ga_2O_3$ from its preferred morphology of rod-like structures to microspheres. The inset of Fig. 1c shows the TEM image of a single microsphere. From the TEM image taken on the surface of the microsphere (Fig. 1c and d) it can be inferred that the microspheres are composed of nanospheres, formed by the aggregation of nanoparticles with average particle size ~85 nm, as also evidenced from the XRD analysis discussed in a later section. These nanospheres are connected densely to each other to form microspheres. The porous nature of the microspheres is due to the interparticle space between the nanospheres. The TEM image taken at the edge of a microsphere shown in the inset of Fig. 1d represents clearly the mesoporous surface of the microsphere. The presence of smaller mesopores facilitates efficient transport of reactant molecules onto the active sites thereby enhancing the efficiency of photocatalysis. The surface properties and distribution of the pores were studied using $N_2$ adsorption–desorption isotherms, as discussed in a later section. The high resolution TEM (HRTEM) image (Fig. 1e) exhibits well-defined lattice fringes with a '*d*'

 

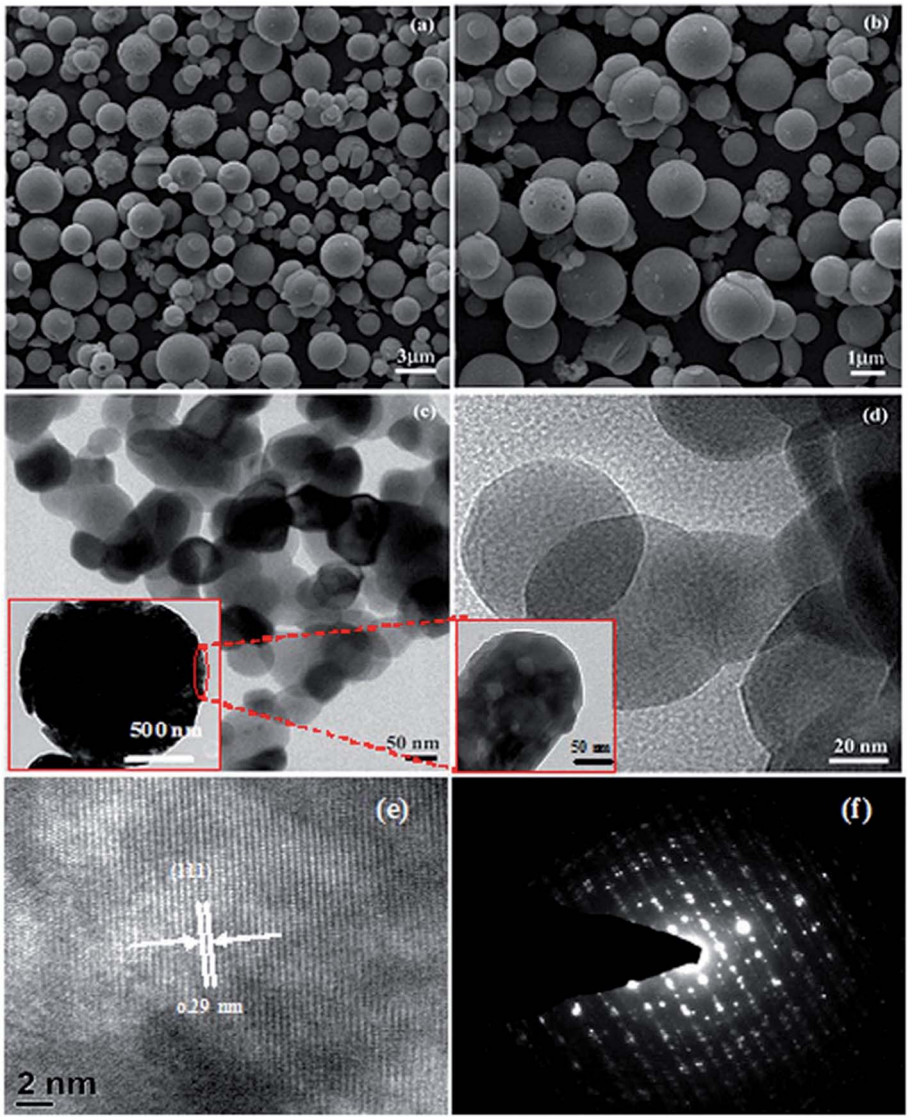


Fig. 1 SEM images of the β-$Ga_2O_3$ microspheres: (a) low magnification;(b) high magnification; (c and d) TEM images of the β-$Ga_2O_3$ microsphere surface (inset of c – single microsphere, d – mesoporous surface); (e) HRTEM; (f) SAED pattern of β-$Ga_2O_3$ microspheres.

space of 0.291 nm, which is consistent with the spacing for a (111) crystal plane of the monoclinic β-$Ga_2O_3$ structure, which explains the broadening of the XRD peak. The selected area diffraction pattern (SAED) in Fig. 1f with discrete spots confirms the single crystalline nature of the β-$Ga_2O_3$ microspheres.

### 3.2 Impact of reaction time and surfactant concentration on the formation of β-$Ga_2O_3$ microspheres

In order to study the morphology evolution of β-$Ga_2O_3$ microspheres, experiments were carried out at various hydrothermal reaction times of 3, 6, 12 and 24 h at a constant temperature of 180 °C. The initial formation of microspheres was observed at 3 h; and the initially or non-uniformly formed microspheres prove that the formation of β-$Ga_2O_3$ microspheres result from the self-assembly process of the nanoparticles as shown in Fig. 2(a). The SEM image for the increased reaction time of 6 h shows that nanoparticles are aggregated in large quantities, tending to form sphere-shaped structures (Fig. 2b). These nanoparticles adhere to the surface of the initially formed microspheres and act as raw materials for the formation of well-defined microspheres in the next stage. As the reaction time was increased to 12 h, well-formed microspheres were obtained and the adhered nanoparticles were found to be consumed as in Fig. 2c. Further when the reaction time was increased to 24 h, the destruction of microspheres starts to take place. Broken microspheres can be observed in Fig. 2d, which indicates the formed microspheres are not hollow which is also revealed from the TEM image of a single microsphere. On the basis of the above discussions it is inferred that, in the initial reaction solution, a group of freestanding crystallites with unequal size in the nonequilibrium state were formed. To lower the total energy of the system, smaller crystallites would eventually dissolve into the solution and regrow the larger ones during the classic Ostwald ripening process.[21] These facts indicate that the

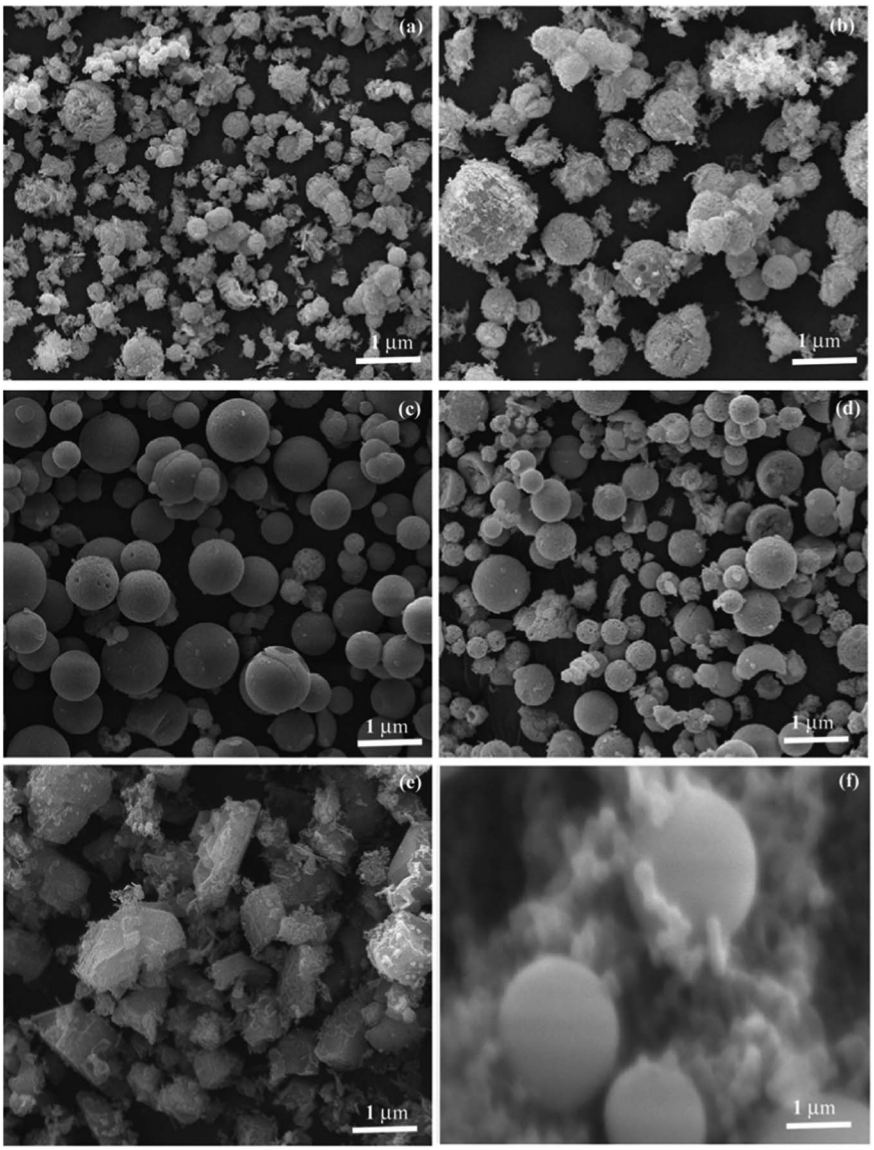


Fig. 2 SEM images of β-$Ga_2O_3$ microspheres: (a) 3 h; (b) 6 h; (c) 12 h; (d) 24 h; (e) low F127 concentration; and (f) high F127 concentration at 180 °C.

formation of β-$Ga_2O_3$ with the microsphere morphology depends on the size of primary particles and also on the reaction time. The ultra-fine particles formed at low reaction times benefit the formation of β-$Ga_2O_3$ microspheres. Morphology analysis indicates that both the morphology and particle size undergo apparent regular changes with hydrothermal reaction time. From the morphological results it is also evident that the crystallinity of microspheres increases with increase in reaction time.

To analyze the effect of the surfactant-to-metal-nitrate concentration on the final form of the β-$Ga_2O_3$ microspheres, we also examined how the molar concentration influenced the morphology of β-$Ga_2O_3$ in the hydrothermal process with a different molar ratio of surfactant to $Ga^{3+}$. The molar concentrations used were (1 : 3), (1 : 5) and (1 : 10), respectively. Agglomerated structures were obtained when the surfactant-to-metal-nitrate solution was (1 : 3) as in Fig. 2e. Meanwhile, with higher concentration (1 : 5), the yield of nanoparticles was higher and highly crystalline intact microspheres were obtained (Fig. 1b). When the concentration was further increased to (1 : 10), few microspheres were formed and a large number of nanoparticles were dispersed throughout. This indicates that an appropriate concentration of surfactant to $Ga^{3+}$ is a crucial prerequisite for the formation of perfect microspheres under the selected reaction conditions. The surfactant F127 absorbed on the surface of the initially formed nanoparticles would direct the self-assembly of nanoparticles by molecular interaction into microspheres with a certain crystallographic orientation. This result is consistent with the observation that the surfactant assisted reaction is a simple and effective way to control the nucleation and growth process.[22,23]

 

### 3.3 Possible formation mechanism of the β-$Ga_2O_3$ microspheres

A plausible formation mechanism of the β-$Ga_2O_3$ microspheres was surveyed systematically by time-dependent reactions and is illustrated schematically in Fig. 3. In the initial stage of the hydrothermal reaction, metal ions in the solution react with pluronic F127 to form relatively stable distorted primary particles of $Ga_2O_3$ under supersaturated conditions, which decreases the free metal ion concentration in the solution and results in the slow generation of primary particles. A homogeneous nucleation process is first initiated. Surfactants are used as morphology directing agents and have a specific mechanism involved in the synthesis of the unique morphology. In the present work, the surfactant pluronic F127 is absorbed by the growing crystal and the growth rate is dependent on the use of an appropriate amount of surfactant and its properties, which control the size and shape of the crystal.[24] The surfactant pluronic F127 form spherical micelles with hydrophobic central cores and hydrophilic chains in the medium. These spherical micelles are used as templates for the formation of β-$Ga_2O_3$ microspheres. Initially, during the hydrothermal reaction, seed crystals are formed. The hydrophilic groups in the pluronic F127 are adsorbed on the surface of the nanoparticles to minimize their surface energy, preventing rapid aggregation of the particles. Consequently, spherical growth of β-$Ga_2O_3$ takes place.

The surfactant molecules evaporate completely during calcination to form very pure mesoporous β-$Ga_2O_3$ microspheres. The formed nanoparticles in the initial stage of the reaction aggregate together, driven by the minimization of interfacial energy.[25] The aggregated nanoparticles act as primary cores that favor homogenous assembly to produce larger self-assembled aggregates *via* self-assembly processes. The aggregated particles tend to form sphere shapes, as the aggregation speed of nanoparticles from each direction to the core is the same. The smaller nanoparticles further dissolve and recrystallize into microspheres in the subsequent hydrothermal growth process *via* self-assembled oriented attachment followed by the Ostwald ripening process. Generally, the Ostwald ripening process involves the formation of aggregates with primary crystallites through a crystallization process due to the energy difference.[26] The effect of reaction time and surfactant concentration on the β-$Ga_2O_3$ microsphere morphology also supports the fact that the Ostwald ripening effect is the essential mechanism. The smooth surface of the microspheres indicates that recrystallization on the surface also accompanies the dissolution process. The evolution steps of the β-$Ga_2O_3$ microspheres are nucleation, growth, dissolution, and recrystallization.


Fig. 3 Schematic illustration of the formation mechanism of β-$Ga_2O_3$ microspheres.

### 3.4 Structural analysis

The phase identity of the β-$Ga_2O_3$ microspheres prepared at a hydrothermal reaction time of 12 h and temperature of 180 °C was determined from the X-ray diffraction pattern shown in Fig. 4(a). The XRD pattern can be indexed to the monoclinic single crystalline phase of β-$Ga_2O_3$ with lattice constants $a = 4.58$ Å, $b = 9.80$ Å and $c = 2.97$ Å within an experimental error of ±0.0003, which is in good agreement with the reported value of β-$Ga_2O_3$ (JCPDS#43-1012).[27] No peaks from the impurities, such as the other phase of $Ga_2O_3$ were found within the detection limit of $2\theta$ in the range 20–80°. The most intense peak (111) indicates the growth direction of the morphology. The average crystallite size was calculated for the prominent plane (111) using Debye–Scherrer formula[21] and was found to be 80 nm. The broadening of the peaks observed could be attributed to the nanometer size of the building blocks, which imply that the lattice distortion in the sample would supply more oxygen vacancies. The sharp and narrow diffraction peaks indicate that the samples have relatively high crystallinity. The spacing of the lattice fringes was 0.29 nm, well indexed with the '*d*' spacing of the prominent plane of the monoclinic β-$Ga_2O_3$ microspheres from the HRTEM image. Hence, the prepared microspheres of β-$Ga_2O_3$ are pure and well crystallized.

Further, the FTIR spectrum of β-$Ga_2O_3$ microspheres was investigated in the range 400 to 4000 $cm^{-1}$, as shown in Fig. 4b from which the functional groups were identified. The peaks around 3444.20 $cm^{-1}$, 2925.27 $cm^{-1}$ and 2851.71 $cm^{-1}$ can be assigned to the stretching vibration of the H–O–H group.[28] The weak bands at 1745.00 $cm^{-1}$ and 1631.45 $cm^{-1}$ represent the stretching vibrations of the O–H groups and bending vibrations of the adsorbed molecular water. The abundance of hydroxyl groups allows the capture of photo-generated holes on the illuminated photocatalyst and forms active hydroxyl radicals, facilitating the decomposition of organic pollutants. The band at about 1020.52 $cm^{-1}$ may be due to the absorption of atmospheric $CO_2$. The strong peak at 665.4 $cm^{-1}$ represents the Ga–O–Ga bending vibration and the peak at 463.97 $cm^{-1}$ can be assigned to the Ga–O bending vibration. The Ga atoms have tetrahedral and octahedral coordination in the lattice. As the lattice of β-$Ga_2O_3$ contains both $GaO_6$ octahedra and $GaO_4$ tetrahedra,[29] it may be assumed that the band at 665.4 $cm^{-1}$ arises due to the vibration of the Ga–O bond in the $GaO_6$ octahedra, while the band at 751.84 $cm^{-1}$ crops up from vibrations in the $GaO_4$ tetrahedra. The FTIR analysis thus gives a clear view

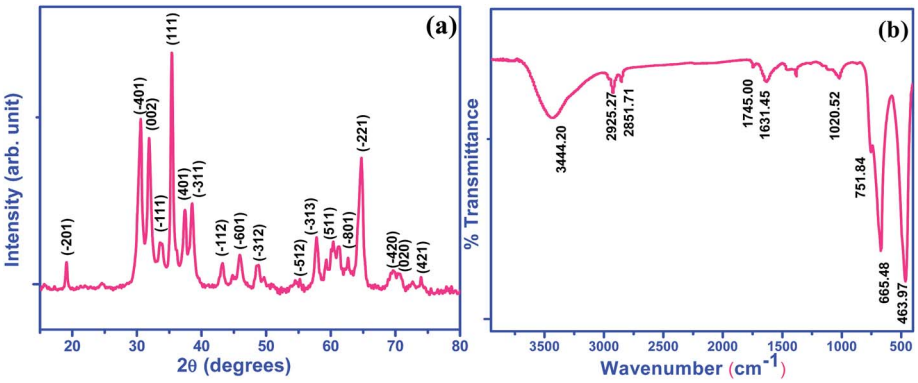


Fig. 4 (a) XRD pattern, (b) FTIR spectrum of β-$Ga_2O_3$ microspheres.

of the presence of only the monoclinic structure of gallium oxide.

### 3.5 Compositional analysis

The compositional analysis of the β-$Ga_2O_3$ nanostructures was carried out using X-ray photoelectron spectroscopy (XPS), a specific spectrometry for chemical analysis of the β-$Ga_2O_3$ surface. The binding energies obtained from the XPS spectrum were corrected with the C 1s reference line at 284.6 eV. A typical XPS survey spectrum with an energy ranging from 0–1200 eV obtained from β-$Ga_2O_3$ microspheres is shown in Fig. 5(a), which reveals the peaks of the core level from Ga 3d, Ga 2p, Ga LLM Auger peak, C 1s, O 1s and O KLL. The energy peaks positioned at 1150.02 and 1122.18 eV, respectively, as in Fig. 5(b), are known to stem from Ga $2P_{1/2}$ and Ga $2P_{3/2}$, representing the Ga–O bonding.[30] The energy peak of Ga 3d centered at 24.26 eV can be ascribed to the presence of gallium in β-$Ga_2O_3$ (Fig. 5c). The O 1s XPS signal observed at a binding energy of 535.12 eV corresponds to the characteristic peak of β-$Ga_2O_3$.[31] The XPS analysis indicates that the material synthesized was β-$Ga_2O_3$, which accords with the XRD measurement. The quantification of peaks reveals that the atomic ratio of Ga–O equals the stoichiometric ratio of 2 : 3. The binding energy values are in agreement with previous reported values.[32]

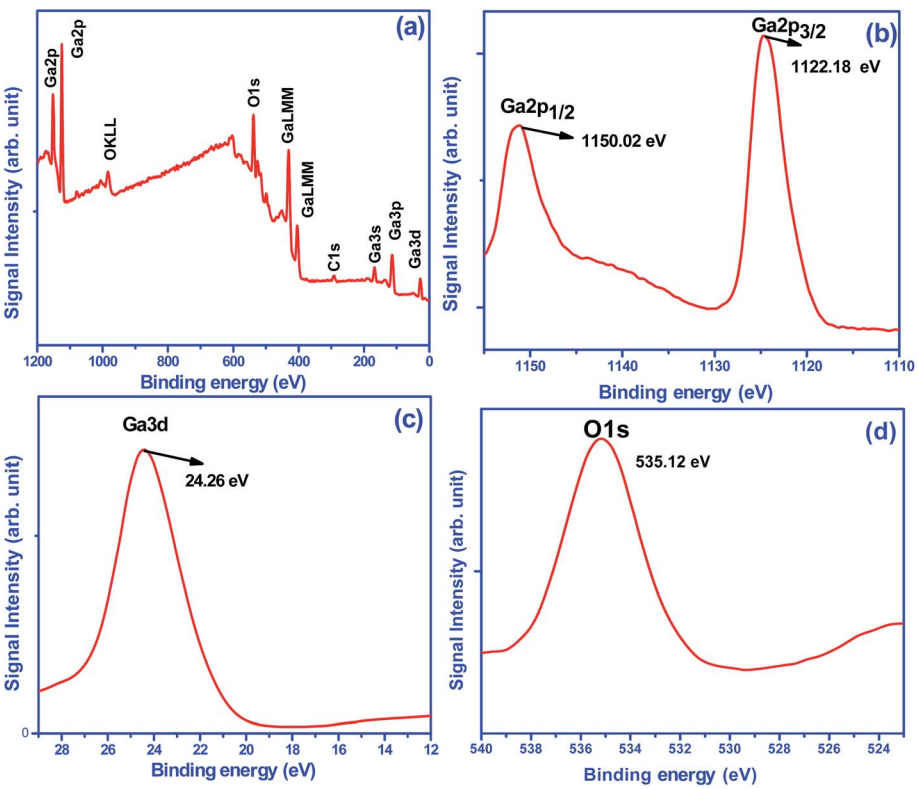


Fig. 5 (a) XPS survey spectrum, (b) Ga 2p, (c) Ga 3d, (d) O 1s of the β-$Ga_2O_3$ microspheres.

 

### 3.6 Optical and specific surface area analysis

The absorption spectrum exhibits a strong absorption feature in the UV region which is characteristic of the electronic transition from the valence band to the conduction band of the β-$Ga_2O_3$ microspheres (Fig. 6a). The diffuse reflectance spectrum of the β-$Ga_2O_3$ allows us to calculate the optical band gap based on the absorption edge using the formula, $E_g = 1240/\lambda_g$.[33] The absorption cut-off wavelength is found to be 276 nm and the corresponding band gap is 4.6 eV. The difference in the absorbance with the reported values could be due to the difference in their morphology, and size.[34] The value of the absorption edge observed for β-$Ga_2O_3$ microspheres prepared by the surfactant assisted hydrothermal process indicates that β-$Ga_2O_3$ nanostructures could serve as a potential photocatalytic material.

It is essential to analyze the surface properties of nanostructures, as they strongly influence the photocatalytic property of the material. Enhanced surface properties can improve the potential of nanostructures in various applications.[35] Hence, the understanding of surface chemistry gains importance. In general, the specific surface area is defined as the ratio between the absolute surface area of a solid and mass. The BET (Brunauer, Emmett and Teller) method involves the determination of the amount of adsorbate required to cover the external and accessible internal pore surfaces of a solid with a complete monolayer of adsorbate. The adsorption isotherm is thus a plot of the amount of gas adsorbed (in mol $g^{-1}$) as a function of the relative pressure. The specific surface area and the corresponding pore size distribution of the β-$Ga_2O_3$ microspheres are determined using the BET and Barrett–Joyner–Halenda (BJH) method. The type IV adsorption–desorption isotherm with an H1 hysteresis loop at a relatively high $P/P_0$ of about 0.9 observed in Fig. 6b, illustrates the mesoporous (2–50 nm) characteristics of the sample, probably formed during the aggregation of nanoparticles to form microspheres composed of nanospheres.[36] The surface area of the prepared β-$Ga_2O_3$ microspheres was found to be 82 $m^2 g^{-1}$. From the BJH method, the pore volume distribution was found to be 0.2 $cm^3 g^{-1}$ (inset of Fig. 6b), relatively higher when compared to the reported values of β-$Ga_2O_3$ synthesized by wet chemical methods.[37] The trace of pores on the surface of microspheres was also observed in the TEM images. The mesopore size distribution of 1–15 nm enhances the decomposition of pollutants by encapsulating the target pollutants on the internal surface of the pores which increases the degradation rate substantially. The porous nature of the microspheres constituted of nanospheres enhances the separation and transfer of photo-induced electron–hole pairs and provides more adsorption sites for the dye molecules, improving the reaction rate during photocatalytic activity.[38] Moreover, the porous structure is believed to facilitate the transportation of reactant molecules and products through the interior space and favors the harvesting of exciting light due to the enlarged surface area and multiple scattering within the pores,[39] useful for photocatalytic application.

### 3.7 Photocatalytic performance of β-$Ga_2O_3$ microspheres for different organic dyes

The heterogeneous photocatalysis is a surface-based process and therefore the relatively large surface area obtained for the β-$Ga_2O_3$ microspheres provides more surface active sites for the adsorption of reactant molecules, which makes the photocatalytic process more efficient.[40]

The photocatalytic degradation towards the dyes Rhodamine B (RhB) and methylene blue (MB) as model pollutants in aqueous solution under ultraviolet (UV) light irradiation has been carried out for the β-$Ga_2O_3$ microspheres constituted of nanospheres. RhB shows a maximum characteristic absorption at $\lambda = 553$ nm, used to monitor the reaction process. The temporal change in the time dependent absorbance spectrum was monitored by examining the variation in maximal absorption spectrum for β-$Ga_2O_3$ microspheres in Fig. 7a.

The absorption peak gradually diminishes as the exposure time to UV irradiation increased, demonstrating the degradation of the dye. RhB was de-ethylated, evidenced by the gradual color change of RhB solution from an intense pink color to almost colorless, revealing the destruction of the chromophoric structure of the dye. Fig. 7c shows the absorption spectrum of MB with a strong characteristic absorption peak at 664 nm. The absorption maximum steadily decreases as the exposure time of ultraviolet light increased to 90 min indicating the process of good adsorption and photodecomposition of the reactive dye. Complete degradation of MB was witnessed at 90 min whereas for RhB dye a longer duration of 180 min was required. The

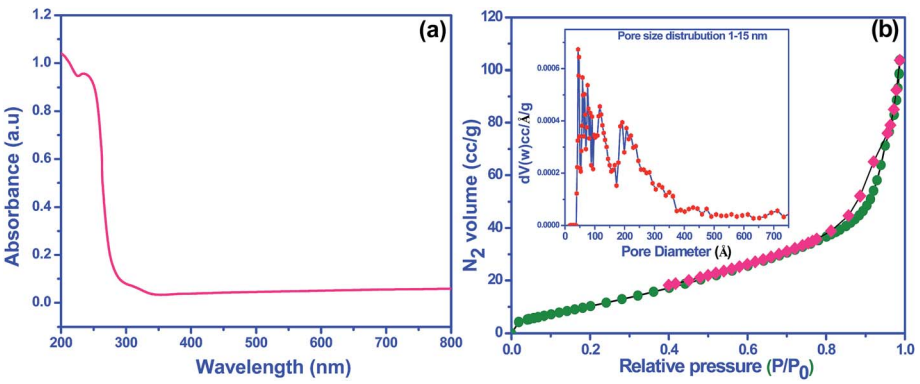


Fig. 6 (a) UV-DRS spectrum, (b) adsorption–desorption isotherm (inset) the corresponding pore size distribution of the β-$Ga_2O_3$ microspheres.

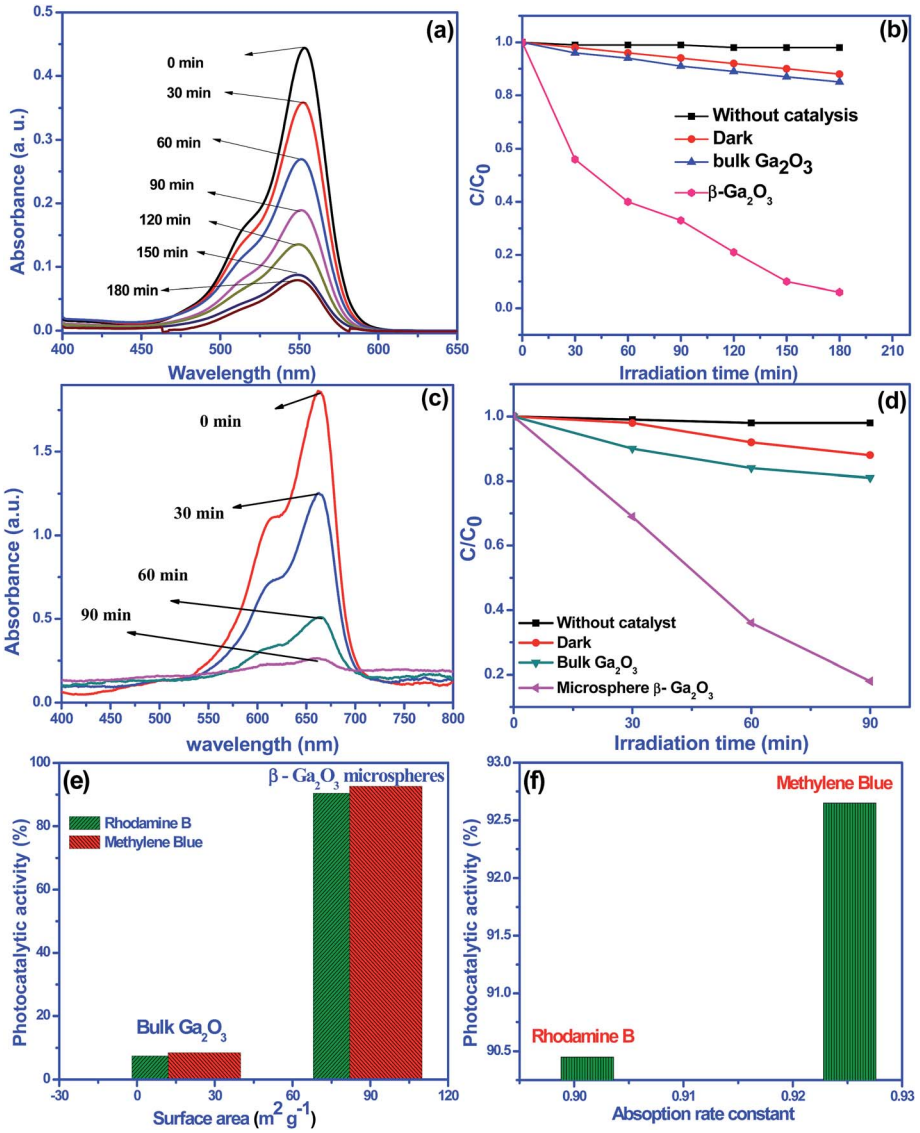


Fig. 7 (a and c) UV-Vis time dependent absorbance spectra during photocatalytic reaction of RhB and MB; (b and d) degradation trend of RhB and MB as a function of irradiation time in the presence of β-$Ga_2O_3$ microspheres; (e) photocatalytic activity *vs.* surface area; and (f) photocatalytic activity *vs.* absorption rate towards RhB and MB for β-$Ga_2O_3$ microspheres.

intense color of the MB solution faded as the irradiation time reached 90 min. The photocatalytic activities of β-$Ga_2O_3$ microspheres differ with respect to the dye used, which may be due to the kinetic differences in the photocatalytic degradation reaction between RhB and MB. The performance of photocatalyst was quantitatively determined by calculating the percentage of degradation; that is, by measuring the relative decrease in the dye concentration against the initial value, by estimating the peak absorbance from the absorption spectrum of the dye solution. The β-$Ga_2O_3$ microspheres comprised of nanospheres are effective catalysts for RhB and MB degradation, as the efficiency was calculated and found to be 90.45 and 92.65%, respectively, using the formula $[(C_0 - C)/C_0] \times 100$, where $C_0$ is the initial concentration and $C$ is the concentration of the dye at time $t$.[41] These results were found to be relatively higher compared to the reported value of β-$Ga_2O_3$ nano/micro structures.[42]

The degradation of RhB and MB as a function of irradiation time for the β-$Ga_2O_3$ microspheres, bulk $Ga_2O_3$, in dark and in the absence of catalyst is shown in Fig. 7(b and d). A blank experiment in the absence of the β-$Ga_2O_3$ microspheres resulted in extremely low photocatalytic decolorization of RhB and MB at about 2–3%. Therefore, the presence of both illumination and the β-$Ga_2O_3$ catalysts were necessary for the efficient degradation of RhB and MB. These results suggest that decolorization of RhB and MB aqueous solution was caused by photocatalytic reactions on the β-$Ga_2O_3$ samples under UV light irradiation and not by the particles adsorbed on the surface. The bulk β-$Ga_2O_3$ shows a lower photocatalytic degradation of ~7.5–8.5% for RhB and MB. The bulk β-$Ga_2O_3$ has a low surface area (12 $m^2$ $g^{-1}$) with no specific morphology when compared to the β-

 

$Ga_2O_3$ microspheres (82 $m^2$ $g^{-1}$). A plot between the photocatalytic activity and the surface area has been presented in Fig. 7e, which implies that the nanostructures have a higher surface area compared to their bulk counterpart, leading to an important role in the enhancement of photocatalytic activity. The $C/C_0$ and irradiation time plot was evaluated and is shown in Fig. 7(b and d). The apparent rate constant[43] was calculated from the plot between $C/C_0$ and irradiation time and was found to be 0.9012 (RhB) and 0.9252 (MB), respectively. These results suggest that the MB dye has a high photocatalytic degradation compared to RhB (Fig. 7f) by using β-$Ga_2O_3$ microspheres comprised of nanospheres as the catalyst, as also suggested by Li-Chia Tien *et al.*[42] Porous photocatalysts have been found to be highly efficient in the photocatalytic decomposition of pollutants.[44] Mesoporous photocatalysts offer a uniform and adjustable environment for encapsulating the target pollutants on the internal surface of the pores, which increases the degradation rate substantially. The β-$Ga_2O_3$ microspheres exhibit high photocatalytic performance as the properties are closely related to the morphology, surface area, band gap energy and pore size distribution. Of these properties, the unique morphology and surface area has an overriding role compared to the other two properties. Different morphologies of β-$Ga_2O_3$ have been reported[9] which exhibit different surface area. In the present case, microspheres of β-$Ga_2O_3$ have a relatively large surface area which provides more surface active sites for the adsorption of reactant molecules, which makes the photocatalytic process more efficient.[40]

The β-$Ga_2O_3$ microspheres comprised of nanospheres were also investigated for their antiphotocorrosion properties. Even after four successive recycles of photodegradation of RhB and MB the catalyst did not exhibit any significant loss of activity as shown in Fig. 8a and b, confirming that β-$Ga_2O_3$ microspheres are not photocorroded during the photocatalytic oxidation of the organic dye molecules.

Several factors such as morphology, particle size, BET surface area and bandgap energy were addressed to understand the photocatalytic activity of the prepared β-$Ga_2O_3$ microspheres constituted by nanospheres. The photocatalytic reaction mechanism involved in the organic dye degradation could be as follows

$$Ga_2O_3 + h\nu \rightarrow Ga_2O_3 + e_{CB}^- + h_{VB}^+$$

$$e_{CB}^- + O_2 \rightarrow O_2^{\bullet -}$$

$$O_2^{\bullet -} + H_2O \rightarrow HO_2^{\bullet} + OH$$

$$HO_2^{\bullet} + H_2O \rightarrow H_2O_2 + OH^{\bullet}$$

$$H_2O_2^{\bullet} \rightarrow 2OH^{\bullet}$$

$$h^+ + OH^- \rightarrow OH^{\bullet}$$

$$OH^{\bullet} + \text{RhB/MB (dye)} \rightarrow CO_2 + H_2O$$

$$h^+ + \text{RhB/MB (dye)} \rightarrow CO_2 + H_2O$$

$$e_{CB}^- + h_{VB}^+ \rightarrow h\nu + \text{recombination (heat)}$$

The reaction mechanism involved during the photocatalytic activities is demonstrated schematically in Fig. 9. During the degradation process, when the catalyst is irradiated with UV

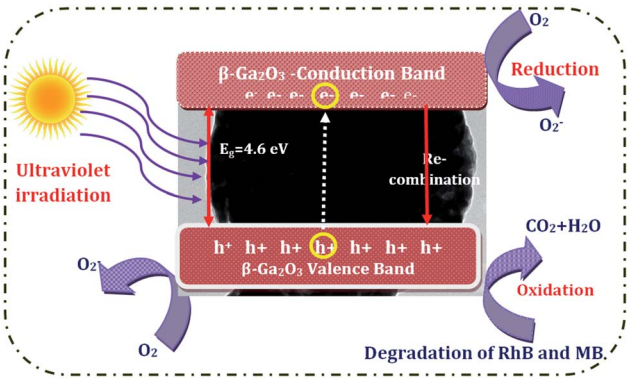


Fig. 9 Schematic illustration of the reaction mechanism involved during photocatalytic activity of β-$Ga_2O_3$ microspheres.

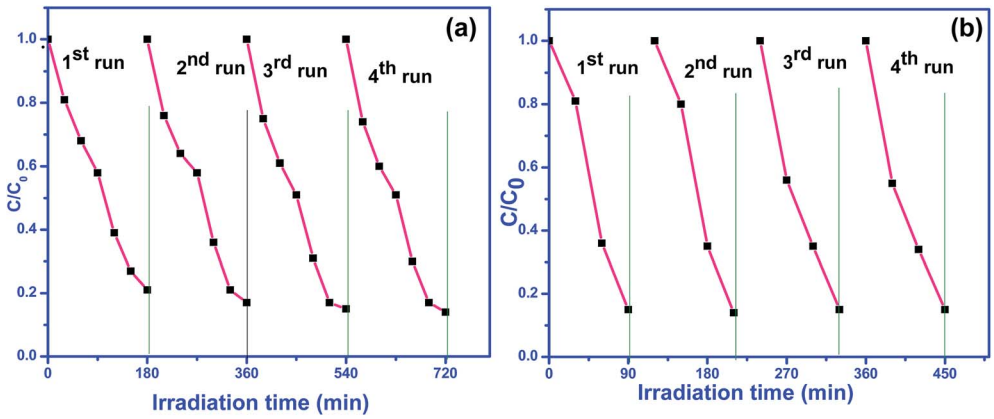


Fig. 8 (a and b) Cyclic photodegradation of (a) RhB and (b) MB.

light having an energy greater than the band gap of the material, the photogenerated electrons are transferred to the conduction band (CB) from the valence band (VB) leaving positive holes in the VB.

The electron–hole pair also produces radiative (light emission), non-radiative (heat or lattice vibrations) recombination or reaction with electron donors and electron acceptors absorbed on the surface. The effective separation of light-induced electrons and holes facilitates their migration to the surface to react with adsorbed reactants. The photoinduced holes in the VB directly oxidize the pollutants, or they are trapped by surface hydroxyl groups at the catalyst surface to yield hydroxyl radicals ($OH^{\bullet}$).[45] These effects improve the oxidizing ability of the nanostructures towards the RhB and MB pollutants. The electrons in the CB are involved in the reduction process, which can be attributed to the band gap and electron–hole pair formation in the VB formed by the hybrid orbitals in the CB. The generated CB electrons react with dissolved oxygen molecules yielding superoxide anion radicals ($O_2^{\bullet -}$) which generate the hydroperoxy radicals ($HO_2^{\bullet}$) on protonation. Further, hydroxyl radicals ($OH^{\bullet}$) are produced by reduction or cleavage of $H_2O_2$ which acts as strong oxidizing agent to decompose the organic dye into non-toxic products.[46] The large surface area and band gap energy of the β-$Ga_2O_3$ microspheres are useful to generate more electron ($e^-$) and hole ($h^+$) pairs. This will prevent the recombination of the $e^-$ and $h^+$, leading to radiationless recombination of the $e^-$ and $h^+$ pairs within the photocatalyst, which will greatly enhance the photocatalytic activity. Furthermore, since the microspheres are composed of nanospheres, the faster the electron–hole pairs arrive at the surface of the catalyst the adsorption rate becomes higher, which favors contact between the material and organic pollutants. This effect also decreases the recombination rate, thereby accelerating the photocatalytic efficiency. It is generally known that for the p-block metal oxide semiconductors, the valence band is usually composed of O 2p orbitals, while the conduction band is composed of the hybridization of s and p orbitals from the p-block metal atom.[47] The dispersive conduction band promotes the mobility of the photogenerated electrons and enhances the charge separation. Beside this, the wide band gap endows the photogenerated charge carriers in the β-$Ga_2O_3$ with strong redox ability. In the proposed photocatalytic degradation mechanism, the higher the specific surface area, the more oxygen molecules were absorbed on the catalyst surface, producing large numbers of $OH^{\bullet}$. On the other hand, the faster the transport of the photogenerated carriers, the more the photocatalytic activity was enhanced. Therefore, the β-$Ga_2O_3$ microspheres composed of nanospheres exhibited enhanced photocatalytic activities towards MB and RhB in the present study.

# 4 Conclusions

A cost effective, facile, surfactant-assisted hydrothermal method to prepare unique β-$Ga_2O_3$ microspheres comprised of nanospheres which act as a photocatalyst has been presented. The effect of reaction time and molar concentration was investigated which exposed the role of these parameters to achieve a controlled and unique morphology. The morphology, particle size (80 nm), band gap energy (4.6 eV) and large surface area (82 $m^2\ g^{-1}$) of the β-$Ga_2O_3$ microspheres influences the photocatalytic activity towards RhB and MB with degradation efficiencies of 90.45 and 92.65%. The photocatalytic ability of β-$Ga_2O_3$ microspheres was high towards MB when compared with RhB. The possible photocatalyst mechanism reveals that $^{\bullet}OH$ radicals in the solution contribute to the degradation reaction along with $O_2^{\bullet -}$ and $H^+$ reactive species. It is concluded from the present work that the β-$Ga_2O_3$ microspheres composed of nanospheres are an economically viable semiconductor metal oxide and a promising candidate with great potential for environment remediation applications.

# Acknowledgements

K. G. gratefully acknowledges DRDO-BU CLS, India for the award of Junior Research Fellow and IACS, India for BET measurement.

# References

1 T. Hari, M. Hodono and I. Komasawa, *Langmuir*, 2000, **16**, 955.
2 J. Zhang, F. Jiang and L. Zhang, *Phys. Lett. A*, 2004, **322**, 363.
3 X. Xiang, C.-B. Cao and He-S. Zhu, *J. Cryst. Growth*, 2005, **279**, 122.
4 F. Zhu, Z. Xue Yang, W. Min Zhou and Ya F. Zhang, *Phys. E.*, 2005, **30**, 155.
5 C. R. Patra, Y. Mastai and A. Gedanken, *J. Nanopart. Res.*, 2004, **6**, 509.
6 G. Guzman-Navarro, M. Herrera-Zaldivar, J. Valenzuela-Benavides and D. Maestre, *J. Appl. Phys.*, 2011, **110**, 034315.
7 K. Girija, S. Thirumalairajan and D. Mangalaraj, *Chem. Eng. J.*, 2014, **236**, 181.
8 Y. Zhao, R. L. Frost and W. N. Martens, *J. Phys. Chem. C*, 2007, **111**, 16290.
9 K. Girija, S. Thirumalairajan, A. K. Patra, D. Mangalaraj, N. Ponpandian and C. Viswanathan, *Semicond. Sci. Technol.*, 2013, **28**, 035015.
10 Y. Zhao, R. L. Frost, J. Yang and W. N. Martens, *J. Phys. Chem. C*, 2008, **112**, 3568.
11 J. Zhang, Z. Liu, C. Lin and J. Lin, *J. Cryst. Growth*, 2005, **280**, 99.
12 B. Pal, M. Sharon and G. Nogami, *Mater. Chem. Phys.*, 1999, **59**, 254.
13 Y. D. Hou, J. S. Zhang, Z. X. Ding and L. Wu, *Powder Technol.*, 2010, **203**, 440.
14 J. Bi, L. Wu, Z. Li, Z. Ding, X. Wang and X. Fu, *J. Alloys Compd.*, 2009, **480**, 684.
15 Y. Hou, X. Wang, Z. Ding and X. Fu, *Environ. Sci. Technol.*, 2006, **40**, 5799.
16 M. Manickavachagam, A. Ramakrishnan, M. S. M. Abdel Wahed, A. Bashir, K. Yasushige, R. P. S. Suri, J. J. Wu and E. T. Sillanpaa, *J. Phys. Chem.*, 2012, **116**, 44.
17 Y. Li, G. Lu and S. Li, *Appl. Catal., A*, 2001, **214**, 179.

 

18 Y. Hou, L. Wu, X. Wang, Z. Ding, Z. Li and X. Fu, *J. Catal.*, 2007, **250**, 12.
19 K. Girija, S. Thirumalairajan, A. K. Patra, D. Mangalaraj, N. Ponpandian and C. Viswanathan, *Curr. Appl. Phys.*, 2013, **13**, 652.
20 V. Srihari, V. Sridharan, H. K. Sahu, G. Raghavan, V. S. Sastry and C. S. Sundar, *J. Mater. Sci.*, 2009, **44**, 671.
21 S. Thirumalairajan, K. Girija, I. Ganesh, D. Mangalaraj, C. Viswanathan and A. Balamurugan, *Chem. Eng. J.*, 2012, **209**, 420.
22 S. Thirumalairajan, K. Girija, V. R. Mastelaro, V. Ganesh and N. Ponpandian, *RSC Adv.*, 2014, **4**, 25957.
23 S. Thirumalairajan, K. Girija, V. R. Mastelaro and N. Ponpandian, *New J. Chem.*, 2014, **38**, 5480.
24 J. Zhou, G. Tian, Y. Chen, J.-Q. Wang, X. Cao, Y. Shi, K. Pan and H. Fu, *Dalton Trans.*, 2013, **42**, 11242.
25 K. Ren, K. Zhang, J. Liu, H. Luo, Y. Huang and X. Yu, *CrystEngComm*, 2012, **14**, 4384.
26 X. Li, Z. Si, Y. Lei, X. Li, J. Tang, S. Song and H. Zhang, *CrystEngComm*, 2011, **13**, 642.
27 A. C. Tas, P. J. Majewski and F. Aldinger, *J. Am. Ceram. Soc.*, 2002, **85**, 1421.
28 U. Rambabu, N. R. Munirathnam, T. L. Prakash, B. Vengalrao and S. Buddhudu, *J. Mater. Sci.*, 2007, **42**, 9262.
29 Y. Quan, D. Fang, X. Zhang, S. Liu and K. Huang, *Mater. Chem. Phys.*, 2010, **121**, 142.
30 Z. F. Zhu, H. J. Sun, H. Liu and D. Yang, *J. Mater. Sci.*, 2010, **45**, 46.
31 H.-D. Xiao, H.-L. Ma, C.-S. Xue, H.-Z. Zhuang, J. Ma, Fu-J. Zong and Xi-J. Zhang, *Mater. Chem. Phys.*, 2007, **101**, 99.
32 X. Shenflin, X. Baojuan and Q. Yitai, *J. Phys. Chem. C*, 2010, **114**, 14029.
33 J. Ding, X. Lu, H. Shu, J. Xie and H. Zhang, *Mater. Sci. Eng., B*, 2010, **171**, 31.
34 S. Xiong, B. Xi and Y. Qian, *J. Phys. Chem. C*, 2010, **114**, 14029.
35 S. Thirumalairajan, K. Girija, N. Y. Hebalkar, D. Mangalaraj, C. Viswantahan and N. Ponpandian, *RSC Adv.*, 2013, **3**, 7549.
36 S. Xiong, B. Xi and Y. Qian, *J. Phys. Chem. C*, 2010, **114**, 14029.
37 W. Zhao, Y. Yang, R. Hao, F. Liu, y. Wang, M. Tan, J. Tang, D. Ren and D. Zhao, *J. Hazard. Mater.*, 2011, **192**, 1548.
38 J. Xi, S. Yin, H. Li, H. Xu, L. Xu and Y. Xu, *Dalton Trans.*, 2011, **40**, 5249.
39 P. Madhusudan, J. Ran, J. Zhang, J. Yu and G. Liu, *Appl. Catal., B*, 2011, **110**, 286.
40 Q. Xiang, J. Yu and M. Jaroniec, *Nanoscale*, 2011, **3**, 3670.
41 J. Yu and L. Qi, *J. Hazard. Mater.*, 2009, **169**, 221.
42 Li-C. Tien, W.-T. Chen and C.-H. Ho, *J. Am. Ceram. Soc.*, 2011, **94**(9), 3117.
43 H. Qi, J. Zhou, Z. Yue, Z. Gui and L. Li, *Mater. Chem. Phys.*, 2003, **78**, 25.
44 M. Muruganandham and Y. Kusumoto, *J. Phys. Chem. C*, 2009, **113**, 16144.
45 H. F. Cheng, B. B. Huang, Y. Dai, X. Y. Qin and X. Y. Zhang, *Langmuir*, 2010, **26**, 6618.
46 X. Zhao and Y. Zhu, *Environ. Sci. Technol.*, 2006, **40**, 3367.
47 K. Ikarashi, J. Sato, H. Kobayashi, N. Saito, H. Nishiyam and Y. J. Inoue, *J. Phys. Chem. B*, 2002, **106**, 9048.